ON THE EFFECT OF AN ANISOTROPY-RESOLVING SUBGRID-SCALE MODEL ON TURBULENT VORTEX MOTIONS

***K. Abe*[1] *and T. Ohtsuka*[1]**

[1] ***Department of Aeronautics and Astronautics, Kyushu University, 744, Motooka, Nishi-ku, Fukuoka 819-0395, Japan***

abe@aero.kyushu-u.ac.jp

1 Introduction

In a large eddy simulation (LES), the flow variables are decomposed into a directly resolved grid-scale (GS) component and an unresolved subgrid-scale (SGS) part that derives from the small-scale eddies. A canonical form of the governing equations for incompressible turbulence may be written as

$$\frac{\mathrm{D}\overline{U}_i}{\mathrm{D}t} = -\frac{1}{\rho}\frac{\partial \overline{P}}{\partial x_i} + \frac{\partial}{\partial x_j}\left\{2\nu S_{ij} - \tau_{ij}\right\}, \qquad (1)$$

$$\frac{\partial \overline{U}_i}{\partial x_i} = 0, \quad S_{ij} = \frac{1}{2}\left(\frac{\partial \overline{U}_i}{\partial x_j} + \frac{\partial \overline{U}_j}{\partial x_i}\right), \qquad (2)$$

where $\overline{(\ )}$ denotes a filtered value. In Eq. (1), ρ, $\overline{P}$, $\overline{U}_i$, ν and S_{ij} denote the density, filtered static pressure, filtered velocity, kinematic viscosity and the strain-rate tensor, respectively. The SGS-stress tensor τ_{ij} is originally expressed as $\tau_{ij} = \overline{U_i U_j} - \overline{U}_i \overline{U}_j$.

LES has long been recognized as a promising way to predict complex turbulence in engineering applications. Since the success of LES depends strongly on the accurate prediction of the SGS stresses, a number of research groups have proposed several kinds of SGS models for τ_{ij} (see for example, Germano et al., 1991; Lilly, 1992; Zang et al., 1993; Vreman et al., 1994; Salvetti and Banarjee, 1995; Horiuti, 1997; Sarghini et al., 1999; Morinishi and Vasilyev, 2001). Although these models have provided encouraging results, there still remain several aspects to be further improved. Among them, an important concern may be in the reduction of the prediction accuracy, when they are applied to engineering applications using coarse grid resolution in the near-wall region.

To overcome this difficulty, Abe (2013) recently proposed a new anisotropy-resolving SGS modeling concept, where the SGS-stress expression is constructed by combining an isotropic eddy-viscosity model (EVM) with an extra anisotropic term (EAT). This SGS model successfully improved the prediction accuracy, particularly with a coarse grid resolution in the near-wall region, while maintaining computational stability. Although the application of the model to several test cases indicated the basic capability of this SGS modeling concept (Abe, 2013; Abe, 2014), it had not been made clear how the EAT worked for improving the predictive performance. To investigate this issue, Ohtsuka and Abe (2013) compared the simulation results obtained by this anisotropic SGS model with those by a linear isotropic SGS model. They found that this anisotropy-resolving SGS model enhanced unsteady motions in the near-wall region.

Based on the above background, the objective of the present study is to elucidate in more detail how the SGS models influence turbulent vortex motions. For this purpose, we perform a detailed investigation of the model performance by means of an *a priori* test using the direct numerical simulation (DNS) data of a plane channel flow. We make several reduced velocity fields from the DNS data with different filter widths. Applying some representative SGS models to these filtered velocity-field data, we evaluate the SGS stresses. The results obtained are compared with the true values estimated directly from the DNS data and the performance of the SGS models is then discussed.

2 Turbulence Models

In what follows, we briefly describe the SGS models investigated in this study.

Conventional linear eddy-viscosity model

The conventional linear EVM has been most often used for LES. Among EVMs, the following two may be representative. One is the Smagorinsky model (SM) (Smagorinsky, 1963) and the other is the dynamic Smagorinsky model (DSM) (Germano et al., 1991; Lilly, 1992). The former is well known to be a model at an early stage of development and the latter is one of the most advanced models in this category.

A canonical form of the linear EVM is expressed as follows:

$$\tau_{ij}{}^{a} = -2\,\nu_{SGS}\,S_{ij}, \qquad (3)$$

where the superscript $(\ )^a$ denotes the anisotropic part of a tensor (i.e., $\tau_{ij}{}^{a} = \tau_{ij} - \tau_{kk}\delta_{ij}/3$). In the Smagorinsky model, the SGS eddy viscosity ν_{SGS} is

modeled as

$$\nu_{SGS} = C_S f_S \Delta^2 \sqrt{2S^2}, \quad f_S = \left\{ 1 - \exp\left(-\frac{y^+}{A} \right) \right\}^2, \tag{4}$$

where $C_S = 0.01\,(= 0.1^2)$ and $A = 25$ are the model constants. In contrast, in the dynamic Smagorinsky model, ν_{SGS} is modeled as follows:

$$\nu_{SGS} = C_S \Delta^2 \sqrt{2S^2}, \tag{5}$$

where the coefficient C_S is locally determined by the dynamic procedure that was originally proposed by Germano et al. (1991), with the aid of the least square approximation by Lilly (1992).

Mixed SGS model

Although introducing a linear EVM into existing CFD codes is easy, a crucial problem has been pointed out: its principal direction does not align with the real SGS-stress tensor. Alternatively, the concept of a "mixed SGS model (mixed model)" may be worth noting. In general, a conventional form of the mixed model can be written as

$$\tau_{ij}{}^a = -2\,\nu_{SGS}\,S_{ij} + (\text{Scale-similarity model})\,. \tag{6}$$

A representative mixed model at an early stage of development is the model proposed by Bardina et al. (1980) as follows:

$$\tau_{ij}{}^a = -2\,\nu_{SGS}\,S_{ij} + \left(\overline{U}_i - \overline{\overline{U}}_i \right) \left(\overline{U}_j - \overline{\overline{U}}_j \right)^a, \tag{7}$$

where the conventional Smagorinsky model is used for ν_{SGS}. Note that considering the summation of the original Leonard term ($\overline{\overline{U}_i \overline{U}_j} - \overline{U}_i \overline{U}_j$) and the modeled cross term ($\overline{\overline{U}}_i(\overline{U}_j - \overline{\overline{U}}_j) + \overline{\overline{U}}_j(\overline{U}_i - \overline{\overline{U}}_i)$) with the model constant being unity due to the restriction of the Galilean invariance, the mixed model in Eq. (7) is rewritten as

$$\tau_{ij}{}^a = -2\,\nu_{SGS}\,S_{ij} + \left(\overline{\overline{U}_i \overline{U}_j} - \overline{\overline{U}}_i \overline{\overline{U}}_j \right)^a. \tag{8}$$

In fact, the second term of this expression coincides with the modified Leonard stress proposed by Germano et al. (1991). In this model, the SGS turbulence energy k_{SGS} may be evaluated as

$$k_{SGS} = \frac{1}{2}\tau_{kk} = \frac{1}{2}\left(\overline{\overline{U}_k \overline{U}_k} - \overline{\overline{U}}_k \overline{\overline{U}}_k \right). \tag{9}$$

Anisotropy-resolving SGS model

In the following, we briefly describe the anisotropy-resolving SGS model proposed by Abe (2013). The SGS stress τ_{ij} in Eq. (1) was modeled as follows:

$$\tau_{ij} = \frac{2}{3}\,k_{SGS}\,\delta_{ij} - 2\,\nu_{SGS}\,S_{ij} + 2\,k_{SGS}\,b_{ij}^{EAT}. \tag{10}$$

In Eq. (10), the anisotropy tensor b_{ij}^{EAT} in the EAT is modeled as

$$b_{ij}^{EAT} = \frac{\tau_{ij}^{'} - \left(-2\nu^{'} S_{ij} \right)}{\tau_{kk}^{'} - (-2\nu^{'} S_{kk})} - \frac{1}{3}\delta_{ij} = \frac{R_{ij}^{'}}{\tau_{kk}^{'}},$$
$$R_{ij}^{'} = \tau_{ij}^{'\,a} - \left(-2\nu^{'} S_{ij} \right). \tag{11}$$

In this model, $\tau_{ij}^{'}$ in Eq. (11) is given by the aforementioned representative scale-similarity model for the SGS Reynolds stress (Bardina et al. (1980)):

$$\tau_{ij}^{'} = \left(\overline{U}_i - \widehat{\overline{U}}_i \right) \left(\overline{U}_j - \widehat{\overline{U}}_j \right), \tag{12}$$

where $\widehat{(\ )}$ denotes a test-filtered value. In Eq. (11), $\nu^{'}$ is an equivalent eddy viscosity evaluated by an EVM-type linear approximation for Eq. (12) as

$$\tau_{ij}^{'\,a} S_{ij} = -2\nu^{'} S_{ij} S_{ij} \;\longrightarrow\; \nu^{'} = -\frac{\tau_{ij}^{'\,a} S_{ij}}{2S^2}, \tag{13}$$

where $S^2 = S_{ij}S_{ij}$. In Eq. (11), $R_{ij}^{'}$ is evaluated by subtracting an EVM form from the original scale-similarity model. Considering the fact that the production term of k_{SGS} is expressed as $-\tau_{ij}\overline{U}_{i,j}$ ($= -\tau_{ij}S_{ij}$), Eq. (13) means that this linearized approximation produces the same amount of energy transfer between the GS and SGS components as the original scale-similarity model. Therefore, $R_{ij}^{'}$ yields no undesirable extra energy transfer between the GS and SGS components; the EAT in Eq. (10) is then expected to properly predict the SGS-stress anisotropy with no serious effect on the computational stability.

Concerning the linear EVM in Eq. (10), this model adopts the one-equation SGS model proposed by Inagaki (2011). The SGS viscosity ν_{SGS} is modeled as follows:

$$\nu_{SGS} = C_{SGS}\,f_{SGS}\sqrt{k_{SGS}}\,\Delta,$$
$$f_{SGS} = 1 - \exp\left\{ -\left(\frac{y_\varepsilon^{'}}{A_0} \right)^{4/3} \right\},$$
$$y_\varepsilon^{'} = \left(\frac{u_\varepsilon y}{\nu} \right) \sqrt{C_l \frac{y}{\Delta}}, \qquad u_\varepsilon = (\nu \varepsilon_{SGS})^{1/4}, \tag{14}$$

where Δ is an SGS filter width. In this study, k_{SGS} and ε_{SGS} are evaluated using the following equations:

$$\frac{\mathrm{D}k_{SGS}}{\mathrm{D}t} = \frac{\partial}{\partial x_j}\left\{ \left(\nu + C_k\,f_{SGS}\sqrt{k_{SGS}}\,\Delta \right) \frac{\partial k_{SGS}}{\partial x_j} \right\} - \tau_{ij}\frac{\partial \overline{U}_i}{\partial x_j} - \varepsilon_{SGS},$$
$$\varepsilon_{SGS} = C_\varepsilon\,\frac{{k_{SGS}}^{3/2}}{\Delta} + \frac{2\nu k_{SGS}}{y^2}. \tag{15}$$

The model constants are as follows:

$$C_{SGS} = 0.05,\;\; A_0 = 30,\;\; C_l = 4,$$
$$C_\varepsilon = 0.835,\;\; C_k = 0.1. \tag{16}$$

More detailed descriptions of this SGS model are given in Abe (2013).

As is found from Eq. (6), a mixed model is originally based on the combination of a linear EVM and a scale-similarity model. With this in mind, the anisotropic SGS model in Eq. (10) is rewritten as

$$\tau_{ij}{}^a = -2\,\nu_{SGS}\,S_{ij} + 2\,k_{SGS}\,b_{ij}^{EAT}. \tag{17}$$

On the other hand, the mixed model in Eq. (8) can be expressed as

$$\tau_{ij}{}^a = -2\,\nu_{SGS}\,S_{ij} + 2\,k_{SGS}\,b_{ij}^{MM}, \tag{18}$$

Table 1: Reduced data for *a priori* tests obtained from the DNS for a channel-flow case.

Case		Re_τ	Grid numbers	Domain (x-z)	Δx^+	Δy^+	Δz^+
C180F	$(\Delta x^+ = 18, \Delta z^+ = 9)$	180	$65 \times 98 \times 65$	$6.4\delta \times 3.2\delta$	18	0.2–9	9
C180M	$(\Delta x^+ = 36, \Delta z^+ = 18)$	180	$33 \times 98 \times 33$	$6.4\delta \times 3.2\delta$	36	0.2–9	18
C180C	$(\Delta x^+ = 72, \Delta z^+ = 36)$	180	$17 \times 98 \times 17$	$6.4\delta \times 3.2\delta$	72	0.2–9	36

where

$$b_{ij}^{MM} = \frac{\left(\overline{\overline{U}_i\overline{U}_j} - \overline{\overline{U}}_i\overline{\overline{U}}_j\right)}{\left(\overline{\overline{U}_k\overline{U}_k} - \overline{\overline{U}}_k\overline{\overline{U}}_k\right)} - \frac{1}{3}\delta_{ij}. \tag{19}$$

Therefore, the anisotropic SGS model by Abe (2013) may be recognized as an alternative version of the mixed model newly introducing an effective correction for stable computation as explained in Eq. (11). In this sense, the model by Abe (2013) can be named the "stabilized mixed model" (SMM, hereafter).

Furthermore, considering the basic concept of the mixed model, another possibility for Eq. (10) may be proposed by using the following scale-similarity model instead of Eq. (12):

$$\tau_{ij}^{'} = \left(\widehat{\overline{U}_i\overline{U}_j} - \widehat{\overline{U}}_i\widehat{\overline{U}}_j\right). \tag{20}$$

In addition, a more advanced version may be available by combining Eq. (12) and Eq. (20) as

$$\tau_{ij}^{'} = C_L\left(\widehat{\overline{U}_i\overline{U}_j} - \widehat{\overline{U}}_i\widehat{\overline{U}}_j\right) + C_B\left(\overline{U}_i - \widehat{\overline{U}}_i\right)\left(\overline{U}_j - \widehat{\overline{U}}_j\right). \tag{21}$$

Note that Eq. (21) is used just for evaluating the SGS-stress anisotropy b_{ij}^{EAT} because k_{SGS} is determined by its transport equation in Eq. (15). Therefore, only the ratio of C_L and C_B is important in this model. Apparently, the combination of ($C_L = 0$, $C_B = 1$) coincides with SMM. Further investigations of this extended anisotropic SGS model will be necessary in future studies.

3 Computational Conditions

Although the basic capability of the SMM was validated by application to some test cases (Abe, 2013; Abe 2014), there still remain several points to be further investigated. In particular, it is important to make clear how the EAT works for enhancing turbulent vortex motions. For this purpose, we performed a detailed investigation of the model performance by an *a priori* test using the DNS data of a plane channel flow at $Re_\tau = 180$ that were originally obtained by Hattori and Nagano (2004). Note that the Reynolds number Re_τ is based on the friction velocity u_τ and the half channel height δ, i.e., $Re_\tau = u_\tau\delta/\nu$. In this study, we made three filtered velocity fields with grid resolutions $(\Delta x^+, \Delta z^+) = (18, 9)$, $(36, 18)$ and $(72, 36)$, where the grid-filter width was set to be the same as the grid spacing of each reduced data, i.e., $\overline{\Delta}_i = \Delta x_i$. Detailed information is summarized in Table 1.

In addition to the *a priori* test, to compare the prediction accuracy of the SGS models, we performed *a posteriori* simulations corresponding to the aforementioned three grid-resolution cases. Note that the computation with the DSM quickly diverged and we thus introduced a well-known strategy of clipping the negative values of ν_{SGS}. Although stable computations were thereby achieved, the effect of the back scatter was no longer included. Moreover, concerning the *a posteriori* calculation with the mixed model, the computation was numerically unstable and results could not be obtained, probably due to the back-scatter effect caused by the scale-similarity model in Eq. (8). Therefore, the investigation of the mixed model was performed only by means of *a priori* test.

A posteriori calculations were performed using an unstructured finite-volume procedure that was the same as that used in Abe (2013), where vertex-centered type storage was used on a grid. For the boundary conditions, the periodic condition was imposed in the streamwise and spanwise directions. On the other hand, the no-slip conditions were specified at the wall surfaces. More detailed descriptions of the computational schemes are given in Abe (2013).

4 Results and Discussion

First, to compare the prediction accuracy of the SGS models for various grid resolutions, we investigate the representative results obtained by *a posteriori* simulations. Figure 1 shows the mean-velocity distributions predicted by the SM and the DSM. It is seen that the accuracy becomes worse as the grid resolution becomes coarser. This trend is a common feature that has been recognized in most of previous studies. In contrast, Fig. 2 shows the results of the SMM. The results of the mean velocity for all grid resolutions correspond fairly well to those of the DNS data. Such a grid-independent trend in the mean-velocity distributions is very encouraging from an engineering viewpoint. The distributions of the total (GS+SGS) Reynolds shear stress also agree well with the DNS data. This fact properly accounts for the prediction accuracy of the mean velocity.

Next, to discuss the fundamental features of the SGS models in more detail, we investigate the results evaluated by *a priori* tests using the DNS data. In the following, due to limitations of space, only the results for C180C will be shown because the effect of an SGS model appears most clearly in the coarsest grid-resolution case. Figure 3 shows the results of *a priori*

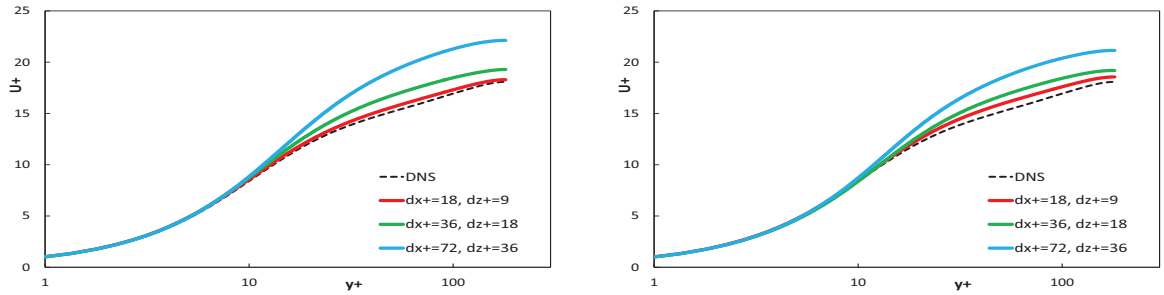

(a) Smagorinsky model (SM) (b) Dynamic Smagorinsky model (DSM)

Figure 1: Mean-velocity distributions predicted by the conventional eddy-viscosity models.

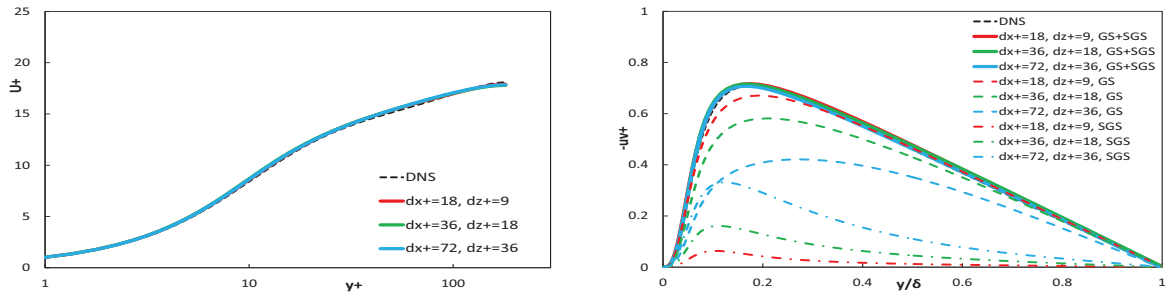

(a) Mean velocity (b) Total (GS+SGS) Reynolds shear stress

Figure 2: Computational results of the present anisotropic one-equation SGS model (SMM).

tests of the conventional eddy-viscosity models, i.e., the SM and the DSM. Note that for these models, we used the true value for k_{SGS} that was directly obtained from the DNS data. Apparently, both models failed to reproduce the SGS normal stresses, obtaining instead an almost isotropic prediction, where each of the SGS normal stresses becomes close to $2k_{SGS}/3$. Although a linear EVM has been widely used, this type of SGS model cannot reproduce the SGS-stress tensor correctly, in particular for its normal components.

In contrast, Fig. 4 shows the results of an *a priori* test of the conventional mixed model (MM, hereafter). For this model, k_{SGS} was evaluated by Eq. (9). Note that the results partially estimated with only the linear EVM term in Eq. (8) are also included. Clearly, the SGS stresses are better predicted particularly for the normal components, although we still see considerable underpredictions. Figure 5 shows the results of an *a priori* test of the SMM. For this model, we used the true value for k_{SGS} because it is originally obtained from the transport equation in a one-equation SGS model. Note that the linear EVM term in Eq. (10) is almost the same as the linear SGS model by Inagaki (2011). As seen in Fig. 5 (a), all components of the SGS stresses are generally predicted well.

That being the case, the SGS models that incorporate the effect of a scale-similarity model, i.e., the MM and the SMM, are found to reproduce the SGS stresses more properly, particularly for the normal components. Considering the fact that the linear part of these SGS models shows a trend similar to the other linear EVMs, it is concluded that a reasonable prediction of the SGS-stress anisotropy is achieved by a scale-similarity model introduced in an SGS model.

In this study, the primary attention is given to the effect of the SGS models on unsteady motions of vortex structures. Taking the curl of Eq. (1) with Eq. (2) yields the following transport equation of the vorticity vector of the filtered velocity:

$$\frac{\mathrm{D}\overline{\omega}_i}{\mathrm{D}t} = \overline{\omega}_j \frac{\partial \overline{U}_i}{\partial x_j} - \varepsilon_{ijk} \frac{\partial}{\partial x_j} \left(\frac{\partial \tau_{kl}}{\partial x_l} \right) + \nu \frac{\partial^2 \overline{\omega}_i}{\partial x_j^2}, \quad (22)$$

where ε_{ijk} is the alternative tensor and the vorticity vector $\overline{\omega}_i$ is defined as

$$\overline{\omega}_i = \varepsilon_{ijk} \frac{\partial \overline{U}_k}{\partial x_j}. \quad (23)$$

In Eq. (22), the first term of the right-hand side is the production term and the third term is the viscous diffusion term. On the other hand, the second term is the SGS-stress term that is expected to give a considerable effect on the predictive performance in LES.

In general, an important concern is how the streamwise vortex structures are enhanced in the near-wall region by the SGS models. Therefore, in what follows, we focus on the instantaneous streamwise-vorticity field (i.e., $\overline{\omega}_x$ for $i = 1$). Its transport equation is expressed as follows:

$$\begin{aligned} \frac{\mathrm{D}\overline{\omega}_x}{\mathrm{D}t} &= \overline{\omega}_x \frac{\partial \overline{U}}{\partial x} + \overline{\omega}_y \frac{\partial \overline{U}}{\partial y} + \overline{\omega}_z \frac{\partial \overline{U}}{\partial z} \quad \text{(Production term)} \\ &+ \frac{\partial}{\partial x} \left(\frac{\partial \tau_{12}}{\partial z} - \frac{\partial \tau_{31}}{\partial y} \right) + \frac{\partial^2}{\partial y \partial z} (\tau_{22} - \tau_{33}) \\ &+ \left(\frac{\partial^2}{\partial z^2} - \frac{\partial^2}{\partial y^2} \right) \tau_{23} \quad \text{(SGS-stress term)} \\ &+ \nu \left(\frac{\partial^2}{\partial x^2} + \frac{\partial^2}{\partial y^2} + \frac{\partial^2}{\partial z^2} \right) \overline{\omega}_x \quad \text{(Viscous term).} \end{aligned} \quad (24)$$

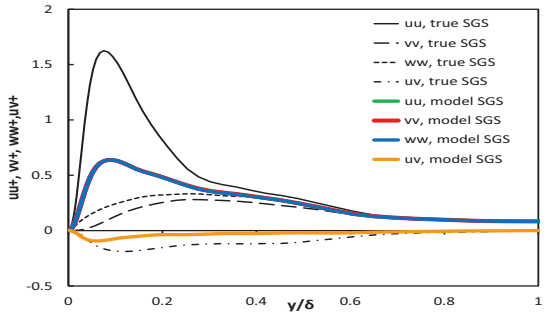

(a) Smagorinsky model (SM)

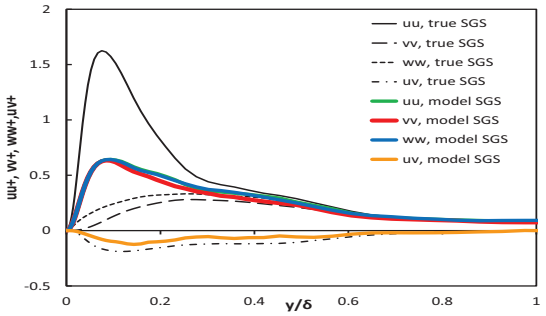

(b) Dynamic Smagorinsky model (DSM)

Figure 3: *A priori* test of the conventional eddy-viscosity models for C180C (k_{SGS} is directly obtained from the DNS data).

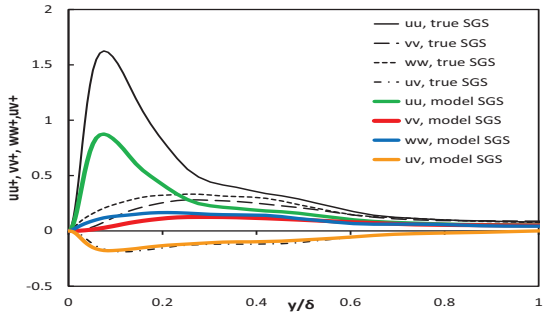

(a) SGS stresses

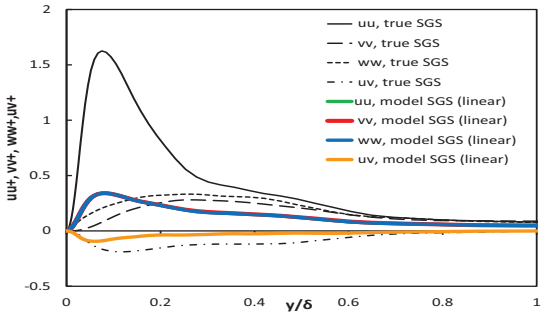

(b) Isotropic (only eddy-viscosity) term

Figure 4: *A priori* test of the conventional mixed model (MM) for C180C (k_{SGS} is evaluated by Eq. (9)).

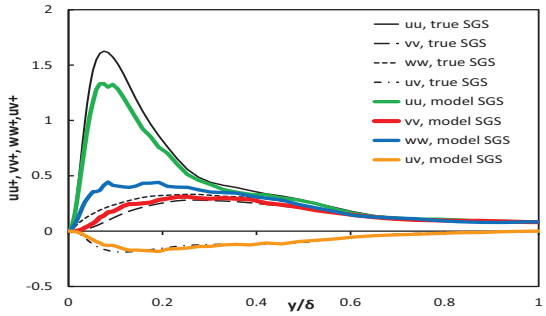

(a) SGS stresses

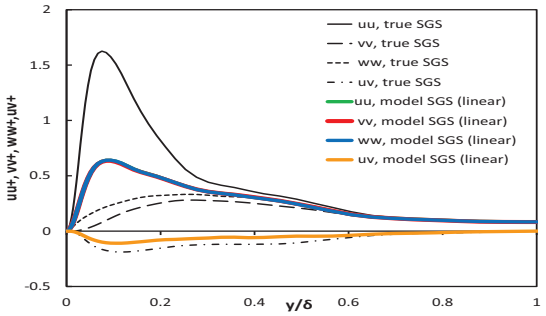

(b) Isotropic (only eddy-viscosity) term

Figure 5: *A priori* test of the anisotropy-resolving SGS model for C180C (SMM: Abe, 2013) (k_{SGS} is directly obtained from the DNS data).

Investigating Eq. (24) gives us valuable information about how the SGS model works in an LES (see for example, Ohtsuka and Abe, 2013). However, we cannot understand easily whether each term works to enhance or reduce the vortex motions because the vorticity has a signed value. Thus, in this study, we multiply the normalized streamwise vorticity to Eq. (24) to make the role of each term clearer. For instance, the modified SGS-stress term ("quasi SGS-stress term", hereafter) is expressed as follows:

$$\left(\frac{\overline{\omega}_x}{|\overline{\omega}_x|}\right)\left\{\frac{\partial}{\partial x}\left(\frac{\partial \tau_{12}}{\partial z}-\frac{\partial \tau_{31}}{\partial y}\right)+\frac{\partial^2}{\partial y \partial z}\left(\tau_{22}-\tau_{33}\right)\right.$$

$$\left.+\left(\frac{\partial^2}{\partial z^2}-\frac{\partial^2}{\partial y^2}\right)\tau_{23}\right\} \quad \text{(Quasi SGS-stress term).} \quad (25)$$

By using Eq. (25), we can understand more easily how the SGS model affects streamwise vortex structures because a positive value of the term means the enhancement of a streamwise vortex motion, and vice versa, regardless of its streamwise rotating direction.

This fact is clearly understood if we investigate the distributions of the viscous term in Eq. (24). Similarly to Eq. (25), the modified viscous term ("quasi viscous term", hereafter) is expressed as

$$\left(\frac{\overline{\omega}_x}{|\overline{\omega}_x|}\right)\left\{\nu\left(\frac{\partial^2}{\partial x^2}+\frac{\partial^2}{\partial y^2}+\frac{\partial^2}{\partial z^2}\right)\overline{\omega}_x\right\}$$

(Quasi viscous term). (26)

Figure 6 compares the results of the original and quasi viscous terms obtained by *a priori* tests using the DNS data for C180C. In Fig. 6 (a), we can see regions in both red and blue colors. Although we recognize that the viscous term works actively near the walls, we can-

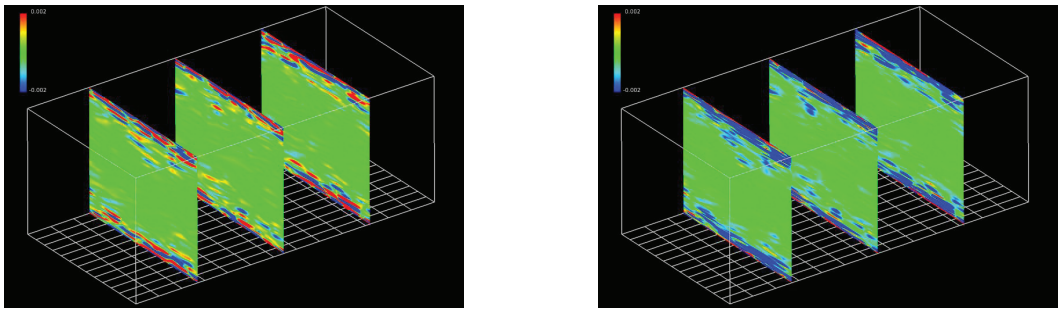

(a) Viscous term (Eq. (24)) (b) Quasi viscous term (Eq. (26))

Figure 6: *A priori* test for original and quasi viscous terms in the streamwise vorticity transport equation using DNS data of Hattori and Nagano (2004) for C180C (color ranges from -2×10^{-3} (Blue) to 2×10^{-3} (Red), all terms are normalized in wall units).

not distinguish whether it works for enhancing or reducing vortex motions. In contrast, it is found from Fig. 6 (b) that the viscous term indeed works almost for reducing the vortex motions because most regions are illustrated in blue, according to Eq. (26).

Figure 7 compares the results of the quasi SGS-stress term in Eq. (25) obtained by an *a priori* test using the DNS data for C180C. In the figure, the predictions by each of the SM, DSM, MM, SMM and the isotropic one-equation SGS model are compared with the strict values directly evaluated from the filtered DNS data. Note that the "isotropic one-equation SGS model" is composed of only the eddy-viscosity term in Eq. (10), which corresponds to Fig. 5 (b).

It is found from the DNS in Fig. 7 (a) that the SGS-stress term basically works for both enhancing and reducing vortex motions. In contrast, as seen in Fig. 7 (b), the SM works almost for reducing the vortex motions because greater part of remarkable regions show the blue color.

Concerning the DSM in Fig. 7 (c), we can see regions in both red and blue colors. Although this fact may imply that the DSM works for both enhancing and reducing vortex motions, it is likely to cause a strong numerical instability in *a posteriori* calculations.

On the other hand, the results of the MM in Fig. 7 (d) look preferable, although the SM is adopted as the linear EVM in Eq. (8). This feature is considered to be achieved by introducing the scale-similarity model. A closer inspection however reveals that the red-color region is not so wide compared with the DNS data.

As seen in Fig. 7 (e), the SMM generally shows a trend similar to that of the DNS, although its effect looks a little too active. It is understood from Fig. 7 (f) that the isotropic one-equation SGS model returns an aspect rather similar to that of the SM. This may be a common feature of this type of conventional linear EVMs. That being the case, it is said that the EAT in the SMM has the capability of enhancing unsteady motions of vortex structures, although it produces no back scatter.

Finally, the computational stability of the SGS models is discussed. Similarly to Eq. (13), an equivalent eddy viscosity ν_E for an SGS stress τ_{ij} is evaluated as

$$\nu_E = -\frac{{\tau_{ij}}^a S_{ij}}{2S^2}. \tag{27}$$

Note that for the conventional EVMs, ν_E is the same as ν_{SGS}. The negative value of ν_E indicates the back scatter where the energy transfers back to the GS component from the SGS component. Thus, by investigating the characteristics of ν_E, we can understand how the back scatter occurs in an LES. We performed *a priori* tests of Eq. (27) for the aforementioned SGS models. Table 2 summarizes the percent fraction of grid nodes at which a negative value of ν_E appears.

First, the true value directly evaluated by the DNS shows a negative value of ν_E in a considerable part for all test cases. This also indicates that there exists the back scatter in real turbulence. In contrast, the SM always returns a positive ν_E that leads to a stable computation, although a strong dissipative feature is seen in the results for coarser grid-resolution cases.

On the other hand, the DSM returns a negative ν_E to reproduce the back scatter. However, it is well known that reproducing the back scatter is likely to cause a strong computational instability. As was described earlier, the present study clipped the negative values of ν_{SGS} in the *a posteriori* tests for stable computation. Thus, the computed results became dissipative and they were rather similar to those by the SM.

As seen in Table 2, Eq. (12) originally generates a negative value of the equivalent eddy viscosity ν' in a considerable part. This type of feature is also seen in another scale-similarity model in the MM and this back-scatter effect still remains even if the stable Smagorinsky model is incorporated. This is considered to be the primary reason why the MM caused a strong numerical instability in an *a posteriori* test.

In contrast, Table 2 shows that the SMM returns no negative ν_E that may cause a computational instability. As was described earlier, the SMM is recognized as an alternative version of the MM newly introduc-

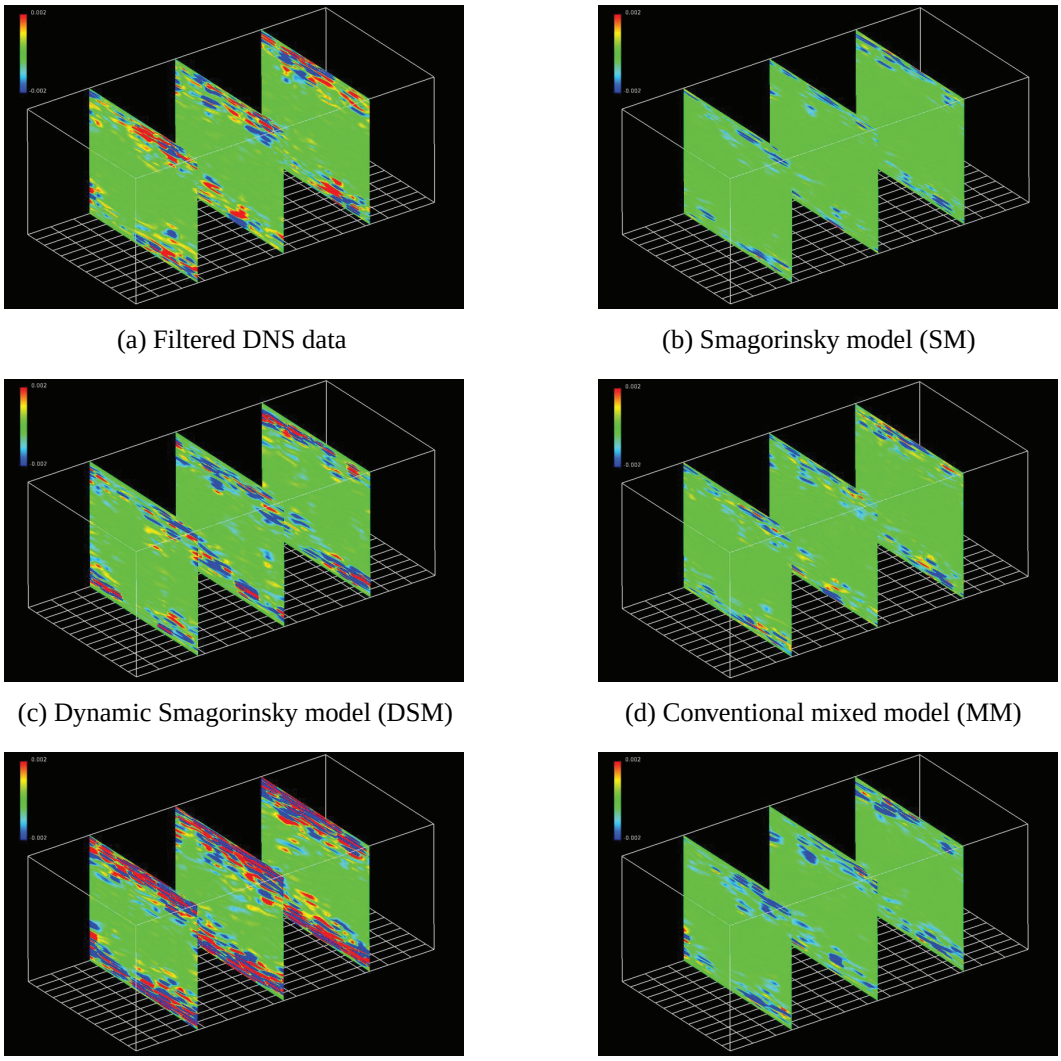

(a) Filtered DNS data

(b) Smagorinsky model (SM)

(c) Dynamic Smagorinsky model (DSM)

(d) Conventional mixed model (MM)

(e) Anisotropic 1-Eq. SGS model (SMM)

(f) Isotropic 1-Eq. SGS model

Figure 7: *A priori* test of quasi SGS-stress term (Eq. (25)) in the streamwise vorticity transport equation using DNS data of Hattori and Nagano (2004) for C180C (color ranges from -2×10^{-3} (Blue) to 2×10^{-3} (Red), all terms are normalized in wall units).

ing an effective correction for stable computation. It is very interesting that the prediction accuracy in *a posteriori* tests is clearly improved for coarser grid-resolution cases, although no back scatter is involved in the calculations.

The SGS-stress term in Eq. (24) plays an important role for enhancing the vortex motions in the near-wall region. As seen in Fig. 7, the effect by the SMM looks very active compared with those of the SM and the isotropic one-equation SGS model. Considering the fact that the SMM returns no negative ν_E, there may exist another key factor besides the reproduction of the back scatter for improving the prediction accuracy under coarser grid-resolution conditions.

5 Concluding Remarks

To elucidate how SGS models influence turbulent vortex motions, we carried out a detailed investigation of the model performance by an *a priori* test using the DNS data of a plane channel flow. We made several reduced velocity fields with different filter widths and then evaluated the SGS stresses by applying some representative SGS models to these filtered data. The results obtained were compared with the true values estimated directly from the DNS data. Furthermore, to illustrate the relation between an SGS model and near-wall vortex structures more clearly, we compared the predicted distributions of the SGS-stress term in the transport equation of the streamwise vorticity ($\overline{\omega}_x$).

It was found that the SM, which is a representative conventional linear EVM, failed to reproduce the SGS normal components at all. Moreover, it worked almost for reducing the turbulent vortex motions because the calculated ν_{SGS} was always positive, resulting in their diffusion. Although the DSM has a possibility of providing a negative ν_{SGS} that implies the back scatter, this model suffered from a strong numerical instability

Table 2: Percent fraction of grid nodes at which negative equivalent eddy viscosity appears for ν_E in Eq. (27).

Model	C180F	C180M	C180C
DNS (true value)	33 %	31 %	27 %
SM (Smagorinsky, 1963)	0 %	0 %	0 %
DSM (Germano et al., 1991; Lilly, 1992)	30 %	27 %	24 %
MM (Bardina et al., 1980)	11 %	11 %	11 %
SMM (Abe 2013)	0 %	0 %	0 %
(for reference)			
$\nu^{'}$ evaluated by Eq. (13) using Eq. (12)	41 %	40 %	39 %

$$\text{Fraction}(\%) = \frac{\text{Number of grid nodes at which negative equivalent eddy viscosity appears}}{\text{Number of total grid nodes}} \times 100$$

and thus needed to clip the negative value for stable computation. Concerning the MM, the *a priori* test indicated a performance better than linear EVMs, while the *a posteriori* calculation was numerically unstable. This instability was also caused by the back-scatter effect that was originally involved in the MM.

In contrast, the SMM, which is an anisotropy-resolving SGS model, showed a notable feature for solving these issues. The *a priori* test confirmed that this model returned the SGS-stress anisotropy properly. This was because the effect of the scale-similarity model was involved, as was similar to the MM. Moreover, this model introduced a modification effective for a stable computation by eliminating the effect of the equivalent EVM from the original scale-similarity model. Interesting is that the SMM still worked for enhancing turbulent vortex motions by means of the effect of the remaining EAT, with which the back scatter was no more produced. Although we understand that the back scatter is an important phenomenon in turbulence, another key factor may exist for improving the predictive performance of an SGS model. Further detailed investigations of this issue will contribute to the development of this research field.

Acknowledgments

This research was supported by a Grant-in-Aid for Scientific Research 24560197, sponsored by the Japan Society for the Promotion of Science. This work was also supported by the "Advanced Computational Scientific Program" of the Research Institute for Information Technology, Kyushu University, Japan. The computation was mainly carried out using the computer facilities at the Research Institute for Information Technology, Kyushu University, Japan. The author wishes to express his appreciation to Professor Y. Nagano and Dr. H. Hattori of the Nagoya Institute of Technology, Japan for the support in using the DNS data.

References

Abe, K. (2013), An improved anisotropy-resolving subgrid-scale model with the aid of a scale-similarity modeling concept, *Int. J. Heat Fluid Flow*, Vol. 39, pp. 42-52.

Abe, K. (2014), An investigation of SGS-stress anisotropy modeling in complex turbulent flow fields, *Flow, Turbulence and Combustion*, Vol. 92, pp. 503-525.

Bardina, J., Ferziger, J.H. and Reynolds, W.C. (1980), Improved subgrid scale models for large eddy simulation, *AIAA Paper*, 80-1357.

Germano, M., Piomelli, U., Moin, P. and Cabot, W.H. (1991), A dynamic subgrid-scale eddy viscosity model, *Phys. Fluids A*, Vol. 3, pp. 1760-1765.

Hattori, H. and Nagano, Y. (2004), Direct numerical simulation of turbulent heat transfer in plane impinging jet, *Int. J. Heat Fluid Flow*, Vol. 25, pp. 749-758.

Horiuti, K. (1997), A new dynamic two-parameter mixed model for large-eddy simulation, *Phys. Fluids*, Vol. 9, pp. 3443-3464.

Inagaki, M. (2011), A new wall-damping function for large eddy simulation employing Kolmogorov velocity scale, *Int. J. Heat Fluid Flow*, Vol. 32, pp. 26-40.

Lilly, D.K. (1992), A proposed modification of the Germano subgridscale closure method. *Phys. Fluids A*, Vol. 4, pp. 633-635.

Morinishi, Y. and Vasilyev, O.V. (2001), A recommended modification to the dynamic two-parameter mixed subgrid scale model for large eddy simulation of wall bounded turbulent flow, *Phys. Fluids*, Vol. 13, pp. 3400-3410.

Ohtsuka, T. and Abe, K. (2013), On the role of an anisotropy-resolving extra term for a subgrid-scale model in near-wall turbulence, *J. Computational Science and Technology*, Vol. 7, pp. 410-425.

Salvetti, M.V. and Banerjee, S. (1995), A priori tests of a new dynamic subgridscale model for finitedifference largeeddy simulations, *Phys. Fluids*, Vol. 7, pp. 2831-2847.

Sarghini, F., Piomelli, U. and Balaras, B. (1999), Scale-similar models for large-eddy simulations, *Phys. Fluids*, Vol. 11, pp. 1596-1607.

Smagorinsky, J. (1963), General circulation experiments with the primitive equations. I. The basic experiment. *Mon. Weather Rev.*, Vol. 91, pp. 99-164.

Vreman, B., Geurts, B. and Kuerten, H. (1994), On the formulation of the dynamic mixed subgrid-scale model, *Phys. Fluids*, Vol. 6, pp. 4057-4059.

Zang, Y., Street, R.L. and Koseff, J.R. (1993), A dynamic mixed subgrid-scale model and its application to turbulent recirculating flows, *Phys. Fluids A*, Vol. 5, pp. 3186-3196.